PARABOLIC SOLAR COOKER DISH: DESIGN AND SIMULATION

Article · January 2011

CITATIONS
4

READS
7,103

1 author:

Dahiru Yahya Dasin
Modibbo Adama University of Technology, Adama
19 PUBLICATIONS **48** CITATIONS

SEE PROFILE

Nigerian Journal of Solar Energy, Vol. 22, 2011 pg. 43-51

PARABOLIC SOLAR COOKER DISH: DESIGN AND SIMULATION

***Dasin, D. Y., **Asere, A. A. and ***Habou, D.**

*Mechanical Engineering Department, Federal University of Technology, Yola.
**Mechanical Engineering Department, Obafemi Awolowo University, Ile Ife.
***Mechanical/Production Engineering Programme, Abubakar Tafawa Balewa University, Bauchi.

*Corresponding Author: dahirudasin@yahoo.com

ABSTRACT

A complete design and simulation of a parabolic dish solar cooker was carried out. The cooker can be used for boiling water as well as cooking in an isolation. A simulation model for transient state was introduced to predict the absorber (cooking pot), pot cover, cooking fluid and air gap temperatures. Linear regression was used to analyzed the data, an average standard error limit of 12.458345% and R^2 of 85.725% for the model was obtained which indicate a satisfactory agreement by comparison of experimental and theoretical result. An average instantaneous efficiency of 84% was determined at beam radiation of 650W/m^2.

Keywords: solar cooker, collector, solar energy, radiation, absorber

INTRODUCTION

The development of solar energy conversion devices and their application is becoming a need these days. The principal motivations of such a concern are the threats of pollution caused by the use of conventional energy sources and the astronomic rise of price of these energy sources, such as oil. Among the techniques of solar energy conversion, the photothermic energy conversion method was found very promising, cheap and consequently easy to develop.

To work at high temperatures, it is necessary to concentrate the incident solar radiation. This could be achieved using collector called solar concentrator. The solar energy concentrating systems comprises of a reflective surface in parabolic form intended to concentrate the solar energy on an absorbing surface, which makes it possible to have a strong increase in heat. The advantage of such a method is to generate high temperatures adapted for heating, solar kitchens and production of electricity by stirling engines. Focusing collectors are designed to produce much higher temperatures than those from flat plate collectors (Habeebullah et al; 1995).

Trial of piping solar energy into kitchens was done by Khalifa et al (1987) as reported by Habou et al (2003), designed two different solar cookers utilizing the heat pipe principle. A cooker utilizing an east –west line focusing collector, designated mecca-1, was developed for this purpose. The second cooker was a flat plate heat pipe cooker Mecca -2. A single heat pipe in each cooker absorbed the energy at the collector, transported it into the kitchen and delivered it to an insulated oven at the condenser end. It was found that mecca-2 cooker with triple glazing had a utilization efficiency of up to 19% and could boil 1 litre of water in 27 min for a solar insolation of 900W/m^2.

An oven that permitted heating from the bottom and sides was developed by Habeebullah et al (1995). This oven consisted of a spiral concentrator and glazed oven placed at the focus. Simulation studies were conducted for predicting the thermal behavior of this cooker for which concentrated solar energy was supplied via a spiral concentrator.

Finally, a parabolic concentrating (point focus) solar cooker has been initiated and its performance simulation is the subject of the present work.

THEORIES RELATED TO PARABOLIC CONCENTRATOR DESIGN

From the equation of parabola, the focal length of the reflector as defined by Rai (2005) is given by,

$$y^2 = 4fx \quad \ldots\ldots\ldots\ldots\ldots\ldots\ldots\ldots\ldots\ldots\ldots\ldots\ldots\ldots (2.1)$$

and $y = \frac{x^2}{4y}$

But from figure 1,

$x = D/2$

Therefore,

$$y = \left(\frac{D}{2}\right)^2 \Big/ _{4f} = D^2 /_{16f} \ldots\ldots\ldots\ldots\ldots\ldots (2.2)$$

The Co-ordinates of point Q are D/2 and $D^2/16f$

$$r = \sqrt{\left(f - D^2/16f\right) + \left(D/2\right)^2 /}$$

$$r = \frac{D^2 + 16f^2}{16f}$$

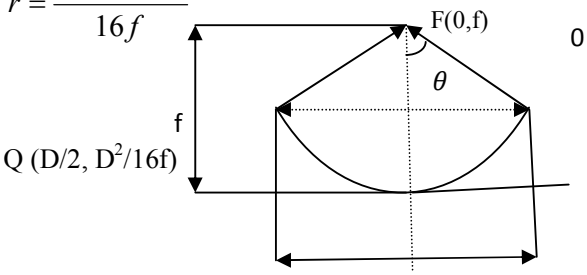

Fig. 2.1: The parabola

And radius of the parabola is given by,

$$r = \frac{2f}{1 + cos\emptyset} \ldots\ldots\ldots\ldots\ldots\ldots\ldots\ldots\ldots\ldots (2.3)$$

□

□□□

$$H = \frac{\pi D^2}{4} \times H_a \ldots\ldots\ldots\ldots\ldots\ldots\ldots\ldots\ldots\ldots\ldots\ldots (2.4)$$

$$D = \left(4H/_{\pi H_a}\right)^{\frac{1}{2}} \ldots\ldots\ldots\ldots\ldots\ldots\ldots\ldots\ldots\ldots (2.5)$$

$$S = \int_{x_1}^{x_2} \sqrt{1 + \left(\frac{dy}{dx}\right)^2}\, dx \ldots\ldots\ldots\ldots\ldots\ldots\ldots\ldots (2.6)$$

$$A = \int_{y_1}^{y_2} 2\pi x \sqrt{1 + \left(\frac{dx}{dy}\right)^2}\, dy \ldots\ldots\ldots\ldots\ldots\ldots 2.7)$$

.

The geometric relationships between a plane of any particular orientation relative to the earth at any time and the incoming solar radiation, that is the position of the sun relative to that plane, can be described in terms of several angles.

The concentration of solar radiation by a parabolic mirror for a target receiver has been theoretically treated on an assumption that the brightness concentration in the solar dish is uniform over the whole area. When the axis of a parabolic mirror is directed towards the sun, the radiation reflected at a point of the mirror spreads as a cone having the same angle as that for the subtended sun, and the axis of the reflected cone always passes through the focal point 'f ' as illustrated in figure 2.1, the rays falling at a point A of the concentrator form an image of the sun on receiver placed at the focus.

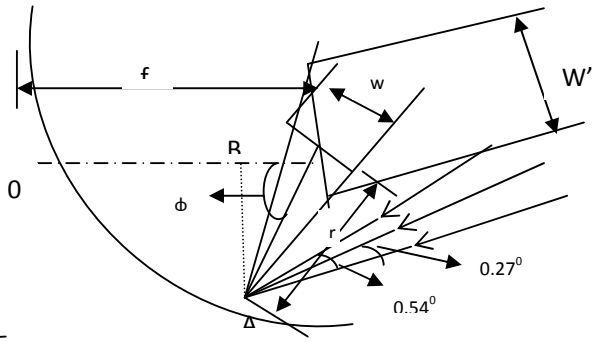

Fig. 2.2, Schematic of Theoretical image formed by a focusing collector

All optical systems form an image of the sun on to the receiver, solar rays have an incline angle of 0.54^0(rim angle) at any point on the earth, because of a very small angle subtended by the sun at any point on earth, a theoretical image created by any optical system will have a finite size depending on the size of the disk and system geometry.

If receiver is planar and normal to the concentrator, the size of the image W' calculated as

$$W' = \frac{2rtan0.27^0}{cos\emptyset} \ldots\ldots\ldots\ldots\ldots\ldots\ldots\ldots\ldots\ldots (2.8)$$

$$W' = \frac{4ftan0.27^0}{(1 + cos\emptyset)cos\emptyset} \ldots\ldots\ldots\ldots\ldots\ldots\ldots\ldots (2.9)$$

As ∅ changes, W' also changes such that

(i) When $\phi = 0$, $W' = 2ftan0.27^0$

(ii) When $\phi = \phi_{max}$

$$W' = \frac{2r_{max}tan0.27^0}{cos\emptyset_{max}} \ldots\ldots\ldots\ldots\ldots\ldots\ldots\ldots\ldots\ldots (2.10)$$

Model Formulation of the Parabolic Solar Cooker

The components of the cooker considered are; the Parabolic Concentrator, the Absorber (Cooking Pot), the Cooking Pot Cover, the Cooking Fluid, and the entrapped air.

The Parabolic Concentrator

For this component, it is considered that the direct component of the beam radiation received

by the reflecting material is reflected to a focus with minimum heat loss which is considered to be negligible.

The Absorber – Cooking Pot

The energy balance for the absorber based on transient condition is,

$$M_a C_a \frac{dT_a}{dt} = Q_{sa} - Q_{cond,a-f} - Q_{conv,a-air} - Q_{rad,a-sky} \quad \text{.....(2.11)}$$

$$Q_{sa} = \alpha\rho A_{conc} I_b F_s + \alpha A_{cyl} I_g \quad \text{.....(2.12)}$$

$$I_g = I_b + I_d \quad \text{.....(2.13)}$$

$$\frac{dT_a}{dt} = 9.9 \times 10^{-3} I_b + 5.6 \times 10^{-2} I_b^{\frac{1}{2}} - 0.045 T_a + 0.039 T_f + 1.08V + 3.6 \times 10^{-3} V T_a - 2.65 \times 10^{-11} - 1.42 \ldots\ldots\ldots\ldots\ldots\ldots\ldots\ldots\ldots\ldots (2.14$$

The Cooking Pot Cover

For the cooking pot cover based on transient condition, the heat balance is correlated as;

$$M_c C_c \frac{dT_c}{dt} = Q_{sc} + Q_{rad,sides-c} - Q_{conv,c-air} - Q_{conv,c-g} - Q_{rad,c-sky} \quad \text{.....(2.15)}$$

Where,

Q_{sc} is the average absorbed energy flux absorbed by the cover.

$$Q_{sc} = \alpha A_c I_g = 95.2\alpha\pi r_c^2 I_b^{\frac{1}{2}} \quad \text{.....(2.16)}$$

$$\frac{dT_c}{dt} = 4.8 \times 10^{-2} I_b^{\frac{1}{2}} - 3.7 \times 10^{-3} T_c + 2.2 \times 10^{-3} T_c V - 0.64V - 4.4 \times 10^{-11} T_c^4 + 4.2 \times 10^{-4} T_g + 9.2 \times 10^{-12} T_a^4 + 1.12 \ldots\ldots\ldots\ldots\ldots\ldots\ldots\ldots (2.17)$$

The Cooking Fluid

For the cooking fluid based on transient condition, the energy balance is,

$$M_f C_f \frac{dT_f}{dt} = Q_{cond,a-f} + Q_{conv,c-g} \quad \text{...(2.18)}$$

$$\frac{dT_f}{dt} = \frac{1.85 \times 10^{-3} T_a}{M_f} - \frac{1.85 \times 10^{-3} T_f}{M_f} + \frac{1.6 \times 10^{-6} T_g}{M_f} \ldots\ldots\ldots\ldots (2.19)$$

The Entrapped Air – Gas

For the entrapped air in the cooking pot, the energy balance based on transient condition is,

$$M_g C_g \frac{dT_g}{dt} = Q_{conv,c-g} + Q_{conv,sides-g} \quad \text{.....(2.20)}$$

$$\frac{dT_g}{dt} = 19T_c - 25.9T_g + 6.7T_a \ldots\ldots\ldots\ldots\ldots\ldots\ldots\ldots\ldots\ldots (2.21)$$

The Computer Simulation

The algorithm was developed based on what Gumel, (2002) suggested and his scheme using Gauss Seidel-type finite difference method adopted for solving the non linear deterministic model.

To circumvent the contrived chaos (and oscillations in numerical results) associated with the use of explicit methods, an easy – to – use derived finite difference method has been constructed to solved the modeling equations.

Starting with the initial value problem for T in equations (2.14), (2.17), (2.19) and (2.21), the development of numerical methods may be based on approximating the time derivative by its first order forward – difference approximant given by,

$$\frac{dT(t)}{dt} = \frac{T(t+l) - T(t)}{l} + 0(l^2) \quad as\ l \to 0, \ldots\ldots\ldots\ldots\ldots\ldots\ldots\ldots\ldots\ldots\ldots\ldots (2.22)$$

Where $l > 0$ is an increment in t (time step). Discretizing the interval $t \geq t_0 = 0$ at the points $t_n = nl(n = 0,1,2, \ldots\ldots)$, the solution at the grid point $x_n\ is\ x(t_n)$.

The solution of an approximating numerical method was denoted by T^n. A first order numerical method for solving T in equations (2.14), (2.17), (2.19) and (2.21) based on approximating the time derivative by equation (2.22) and making appropriate approximations for the right hand side terms, is

$$M_{T_a}: \frac{1}{l}\left({T_a}^{n+1} - {T_a}^n\right) = \pi - \mu {T_a}^{n+1} - \frac{\beta_1 c {T_a}^{n+1} T_c^n}{{T_a}^n + T_c^n + T_f^n + T_g^n} - \frac{\beta_2 c {T_a}^{n+1} T_f^n}{{T_a}^n + T_c^n + T_f^n + T_g^n} \ldots\ldots\ldots (2.23)$$

Similarly, the methods for $T_c, T_f \ and \ T_g$ are respectively given by,

$$M_{T_c}: \frac{1}{l}(T_c^{n+1} - T_c^n) = \frac{\beta_1 c T_a^{n+1} T_c^{n+1}}{T_a^{n+1} + T_c^n + T_f^n + T_g^n} - (\mu + \gamma_1 + \tau) T_c^{n+1} \ldots\ldots\ldots\ldots (2.24)$$

$$M_{T_f}: \frac{1}{l}\left(T_f^{n+1} - T_f^n\right) = \frac{\beta_2 c T_a^{n+1} T_f^{n+1}}{T_a^{n+1} + T_c^{n+1} + T_f^n + T_g^n} - (\mu + \gamma_2 + \tau) T_f^{n+1} \ldots\ldots\ldots\ldots\ldots\ldots (2.25)$$

$$M_{T_g}: \frac{1}{l}\left(T_g^{n+1} - T_g^n\right) = \frac{\beta_3 c T_a^{n+1} T_g^{n+1}}{T_a^{n+1} + T_c^{n+1} + T_f^{n+1} + T_g^n} - (\mu + \gamma_3 + \tau) T_g^{n+1} \ldots\ldots\ldots\ldots\ldots\ldots (2.26)$$

Following Gumel (2002), the time-step, l, in (2.23) – (2.26) is approximated by

$$l = \Delta t \rightarrow \frac{1 - e^{-2l}}{2} \ldots\ldots\ldots\ldots\ldots\ldots\ldots\ldots\ldots\ldots (2.27)$$

This approximations is important in ensuring that the numerical results is free of contrived chaos and oscillations.

Rearranging the methods (2.23) – (2.26) and noting (18) gives

$$T_a{}^{n+1} = (T_a^n + \pi \Delta t) \Big/ \left\{1 + \Delta t \left[\mu + \frac{c}{T_a^n + T_c^n + T_f^n + T_g^n}\left(\beta_1 T_c^n + \beta_2 T_f^n\right)\right]\right\} \ldots\ldots\ldots\ldots (2.28)$$

$$T_c^{n+1} = T_c^n \Big/ \left\{1 + \Delta t \left(\mu + \gamma_1 + \tau - \frac{\beta_1 c T_a^{n+1}}{T_a^{n+1} + T_c^n + T_f^n + T_g^n}\right)\right\} \ldots\ldots\ldots\ldots\ldots\ldots\ldots\ldots (2.29)$$

$$T_f^{n+1} = T_f^n \Big/ \left\{1 + \Delta t \left(\mu + \gamma_2 + \tau - \frac{\beta_2 c T_a^{n+1}}{T_a^{n+1} + T_c^{n+1} + T_f^n + T_g^n}\right)\right\} \ldots\ldots\ldots\ldots\ldots\ldots\ldots\ldots (2.30)$$

$$T_g^{n+1} = T_g^n \Big/ \left\{1 + \Delta t \left(\mu + \gamma_3 + \tau - \frac{\beta_3 c T_a^{n+1}}{T_a^{n+1} + T_c^{n+1} + T_f^{n+1} + T_g^n}\right)\right\} \ldots\ldots\ldots\ldots\ldots\ldots\ldots (2.31)$$

The temperatures of all the components of the cooker were initialized at an ambient temperature of 302^0K corresponding to the time when the cooker was set under the sun. The values of the beam radiation, wind speed and mass of cooking fluid were the input parameters for the simulation. The temperature distribution of all the components of the cooker were obtained by solving the energy balance equations (2.14), (2.17), (2.19) and (2.21) numerically using the algorithm developed by Gumel (2002).

RESULTS AND DISCUSSIONS

A Computer simulation for the cooker was prepared to predict the temperatures of the various points of the cooker for each period of operation. These are, the predicted temperature for absorber (cooking pot), pot cover, cooking fluid and air gap. Tabulated in Tables (1) – (4) and plotted in Figures (1) – (4), are the predicted and experimental results of cooking fluid temperature for comparison. From the theoretical result it was found that cooking fluid of 0.522kg reaches a boiling temperature of 94.2^0C after 1hour 15 minutes at beam radiation of 623.1W/m^2 and wind speed of 0.9 m/s, this can be compared with experimental result in which the cooking fluid boil at almost the same time but due to practical situation of convective heat losses as a result of wind speed fluctuation during experiment, it was a little bit longer than the testing result. When the beam radiation was varied as shown on figure 2 for the theoretical result to 507.7 W/m^2, and wind speed of 1.3m/s, at the same mass of cooking fluid of 0.522Kg, the boiling temperature of cooking fluid was found to be 94.1^0C after 1hour 15minutes, the experimental result for this was found that the boiling temperature of the cooking fluid was 89^0C after just 1hour 30minutes due to practical

conditions. Figure 3 is for the theoretical result at beam radiation of 540W/m^2, 1Kg mass of cooking fluid and wind speed of 0.98 m/s, the boiling temperature was found to be 95.3^{0}C after 2hours 15 minutes, but from the experimental result at the same weather condition the boiling temperature of 95^{0}C was found at exactly 1 hour due to calm weather condition. Figure 4, shows a comparison of theoretical results with experimental result which indicates that lower temperature was recorded for the theoretical result due clear weather condition during testing period.

Figure 5, shows theoretical cooking fluid temperature variation at different mass of fluid with constant beam radiation of 450W/m^2, from the figure it indicates that as the mass increases the boiling time increases. Figure 6, shows the instantaneous efficiency of the cooker with time, it shows that at the onset of the cooking the efficiency is high, but with time it continue to decline due to increase in heat loss as a result of temperature increase. An average efficiency of 84% was determined at beam radiation of 650W/m^2. Linear regression was used to analyzed the data, an average standard error limit of 12.458345% and $R^2$of 85.725% for the model was obtained which indicate a satisfactory agreement by comparison of experimental and theoretical result.

CONCLUSION

A predicted temperature at various component of the cooker was obtained, that is absorber (cooking pot), pot cover, cooking fluid and air gap temperature. From the predicted results it is evidently clear that this cooker can substitute the traditional method of cooking using other conventional means. It took less cooking time under clear weather condition to boil 1 kg of fluid as shown in the figures above, peak temperature of 95^{0}C was obtained in just 1 hour which can compute well with other conventional sources. Correlation between theoretical and experimental results carried out using linear regression analysis indicate satisfactory result.

Nomenclature

A_{cyl} = Area of the cylindrical section of absorber (m)
A_{conc} = Area of the concentrator (m)
C_a = Specific heat of the absorber (KJ/Kg^{0}K)
C_c = Specific heat of the pot cover (KJ/Kg^{0}K)
C_g = Specific heat of the gas (air gap) (KJ/Kg^{0}K)
C_f = Specific heat of the cooking fluid (KJ/Kg^{0}K)
F_s = $1 - \frac{A_{sh}}{A_c}$ = Shading factor of the pot.
f = focal length of the parabola (m)
I_b = Beam radiation (W/m^2)
I_g = Global Radiation (W/m^2)
M_a = Mass of the absorber (Kg)
M_c = Mass of the pot cover (Kg)
M_g = Mass of the gas (air gap) (Kg)
M_f = Mass of the cooking fluid (Kg)
n = Average day of the Month, rotation the earth on its axis at 15^0 per hour.
r = Radius of the Parabola (m)
T_a = Temperature of the absorber (^{0}K)
T_c = Temperature of the pot cover (^{0}K)
T_f = Temperature of the cooking fluid (^{0}K)
T_g = Temperature of the gas (air gap) (^{0}K)

V	=	Wind speed (m/s)
W'	=	Size of the Image formed at the focus (m)
α	=	Absorptivity of the absorber (cooking pot)
ρ	=	Reflectivity of the reflecting material
ϕ	=	Angle between the axis and the reflected beam at the focus (rim angle)
θ	=	Angle of incidence, the angle between the beam radiation on a surface and normal to that surface.
β	=	Slope, the angle between the plane surface in question and that horizontal.
γ	=	Surface azimuth angle, the deviation of the projection on a horizontal plane of the normal to the surface from the local meridian.
ω	=	Hour angle, the angular displacement of the Sun east or west of the local meridian due to.

Subscript

a	=	absorber
b	=	beam
c	=	cover
g	=	air gap
f	=	fluid

REFERENCES

Duffie J. A. and Beckman W. A. (1974), Solar engineering of thermal processes, John Wiley and Sons, New York.

Gumel A.B.; A Competitive Numerical Method for a Chemotherapy Model of Two HIV Subtypes. *Journal of applied Mathematics and Computation,* Vol. 131, Pp 329-337.

Habeebulah, M. B., Khalifa, A. M. and Olwi, I., (1995), The Oven receiver, an approach toward the revival of concentrating Solar cookers, *International Journal of solar energy,* Vol. 54 No. 4 pp 227 – 237.

Habou, D., Asere, A.A. and Sambo, A.S., (2003), Simulation on the Performance of 2X-CPC Solar Cooker, *Nigerian Journal of Tropical Engineering,* Vol. 4 Nos. 1&2, Pp. 41-48.

Khalifa, A.M., Taha, M.M.A. and Kyurt, M., (1987), Design Simulation and Testing of a new concentrating type solar cooker, *International Journal of Solar Energy,* Vol. 38. Pp. 79-88.

Rai, G.D., (2005), Solar Energy Utilization, Khanna Publishers, Nai Sarak Delhi, Pp. 202-206.

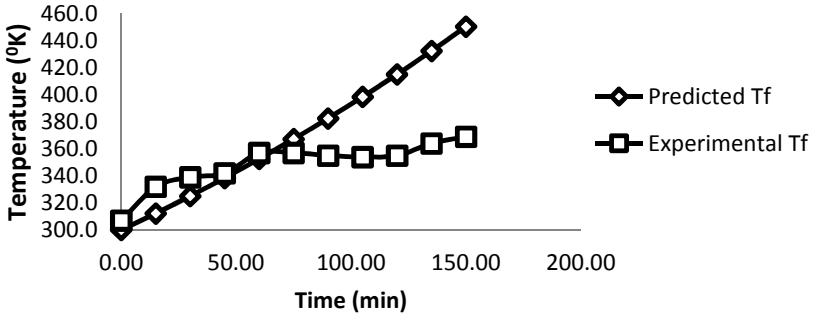

Fig. 1, Theoretical and Experimental Temperature Distribution for beam radiation of 623.1 W/m², mass of cooking fluid 0.522Kg and 0.9M/s wind speed

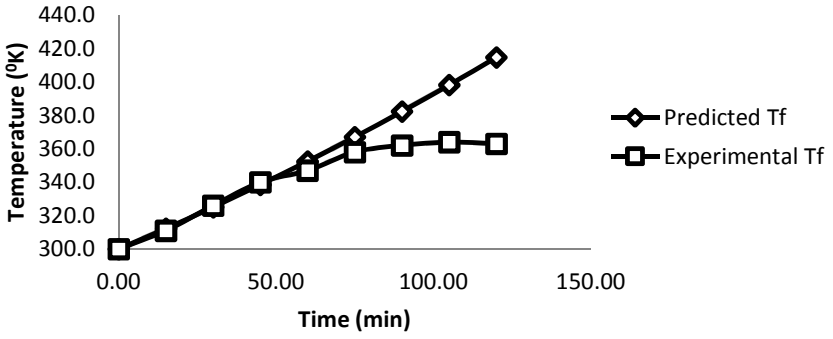

Fig. 2, Theoretical and Experimental Temperature Distribution for beam radiation of 507.7 W/m^2, mass of cooking fluid 0.522Kg and 1.3m/s wind speed

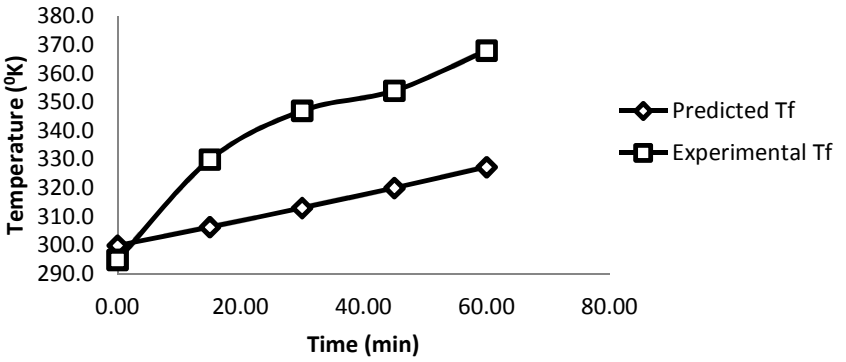

Fig. 3, Theoretical and Experimental Temperature Distribution for beam radiation of 540 W/m^2, mass of cooking fluid 1Kg and 0.98m/s wind speed

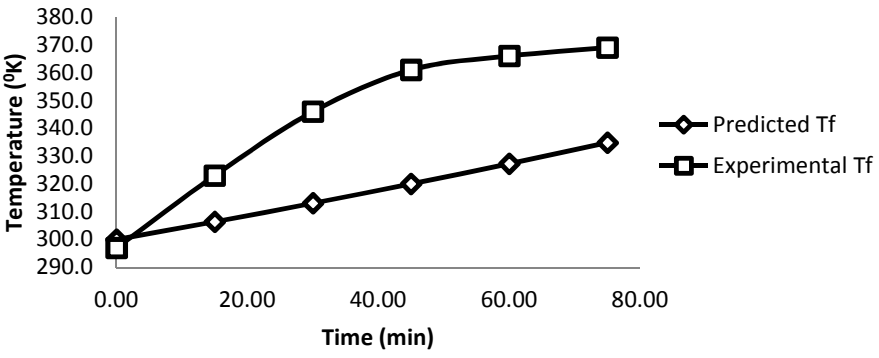

Fig. 4, Theoretical and Experimental Temperature Distribution for beam radiation of 484.6 W/m^2, mass of cooking fluid 1Kg and 0.7m/s wind speed

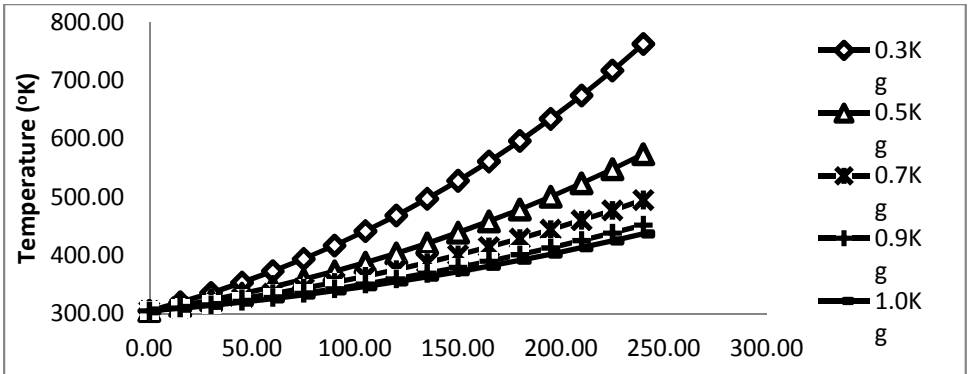

Fig.5; Predicted result of Cooking Fluid Temperature Distribution for I_b = 450W/m² at Various Mass of Fluid

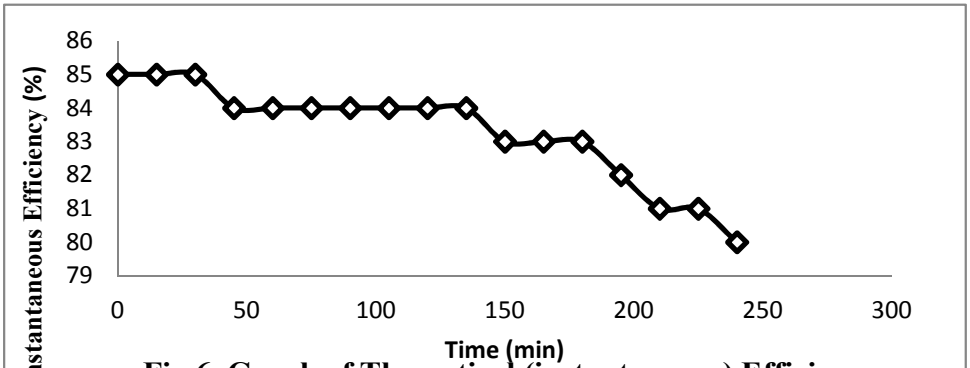

Fig.6, Graph of Theoretical (instantaneous) Efficiency with Time at I_b = 650w/m²

Table 1: Theoretical and Experimental Temperature Distribution at Various Point of Cooker

		Predicted			
Time (min)	**Experimental (T_f)**	**T_a(^{0}K)**	**T_c ^{0}K)**	**T_f (^{0}K)**	**T_g(^{0}K)**
0.00	307	300.0	300.0	300.0	300.0
15.00	332	316.1	305.4	312.3	305.0
30.00	339	332.6	310.9	325.1	312.9
45.00	342	349.5	316.4	338.5	321.2
60.00	357	366.8	322.0	352.6	329.8
75.00	357	384.6	327.7	367.2	338.6
90.00	355	402.9	333.5	382.5	347.5
105.00	354	421.7	339.4	398.5	356.7
120.00	355	441.0	345.4	415.1	366.0
135.00	364	460.9	351.5	432.4	375.6
150.00	369	481.3	357.7	450.5	385.4

wind speed 0.9m/s, beam radiation 623.1 W/m^2
mass of cooking fluid 522g

Table 2: Theoretical and Experimental Temperature Distribution at Various Point of Cooker

		Predicted			
Time (min)	**Experimental (T_f)**	**T_a(^{0}K)**	**T_c (^{0}K)**	**T_f (^{0}K)**	**T_g(^{0}K)**
0.00	300	300.0	300.0	300.0	300.0
15.00	311	315.8	305.3	312.3	304.9
30.00	326	332.0	310.6	325.1	312.5
45.00	340	348.6	316.0	338.5	320.7
60.00	347	365.7	321.5	352.5	329.1
75.00	358	383.3	327.0	367.1	337.7
90.00	362	401.3	332.7	382.3	346.5
105.00	364	419.8	338.4	398.2	355.5
120.00	363	438.9	344.2	414.8	364.7

wind speed 1.3m/s, beam radiation 507.7 W/m^2
mass of cooking fluid 522g

Table 3: Theoretical and Experimental Temperature Distribution at Various Point of cooker

		Predicted			
Time (min)	**Experimental (T_f)**	**T_a(^{0}K)**	**T_c ^{0}K)**	**T_f (^{0}K)**	**T_g(^{0}K)**
0.00	295	300.0	300.0	300.0	300.0
15.00	330	315.8	305.3	306.4	304.9
30.00	347	331.7	310.6	313.1	312.5
45.00	354	347.7	316.0	320.1	320.5
60.00	368	363.9	321.5	327.3	328.7

wind speed 0.98m/s, beam radiation 540 W/m^2
mass of cooking fluid 1Kg

Table 4: Theoretical and Experimental Temperature Distribution at Various Point of cooker

		Predicted			
Time (min)	**Experimental (T_f)**	**T_a(^{0}K)**	**T_c ^{0}K)**	**T_f (^{0}K)**	**T_g(^{0}K)**
0.00	297	300.0	300.0	300.0	300.0
15.00	323	315.4	305.1	306.4	304.7
30.00	346	330.8	310.3	313.1	312.1
45.00	361	346.5	315.5	320.0	319.9
60.00	366	362.2	320.8	327.3	327.8
75.00	369	378.2	326.2	334.8	335.9

wind speed 0.7m/s, beam radiation 484.6W/m^2
mass of cooking fluid 1Kg